Progress In Electromagnetics Research M, Vol. 21, 33–45, 2011

INTERFEROMETRIC ISAR THREE-DIMENSIONAL IMAGING USING ONE ANTENNA

C. L. Liu*, X. Z. Gao, W. D. Jiang, and X. Li

College of Electronic Science and Engineering, National University of Defense Technology, Changsha 410073, China

Abstract—Conventional interferometric ISAR (InISAR) imaging requires a radar system with at least three antennas, and the hardware complexity may be a main obstacle to practical realization. In this paper, we propose an InISAR three-dimensional imaging algorithm using only one antenna. Interferometric processing is carried out among ISAR images obtained during three near measurement intervals. The scatterer position in the range direction is obtained from range cell number in ISAR images, and the azimuth/height information is estimated from interferometric phases and geometrical relationship. Moreover, the target track requirements of the proposed method are also investigated. Simulations have shown the effectiveness of the proposed method.

1. INTRODUCTION

Three-dimensional (3-D) images are capable of providing a more reliable description of target features, which is advantageous to target identification. Therefore, high-resolution 3-D radar imaging has become a promising technique in the radar signal processing community [1, 2]. Applying the multi-antenna interferometric technique to ISAR imaging, we have interferometric inverse synthetic aperture radar (InISAR) [3], which produces a 3-D image of the target. The traditional InISAR imaging requires a radar system with at least two receiving antennas spatial-separately equipped along a baseline. The echoes from the target are simultaneously received by the two receivers and are processed to obtain two two-dimensional (2-D) range-Doppler images via the conventional ISAR imaging algorithm. The azimuth/height

Received 8 July 2011, Accepted 18 September 2011, Scheduled 21 September 2011

* Corresponding author: Chenglan Liu (liuchenglan2010@163.com).

information is estimated from phase differences of the same scatterer in the two 2-D images. Together with the radial information, a 3-D image consistent with the real target is obtained accordingly [4, 5].

InISAR imaging has been widely investigated [4–13]. However, it costs large for adding two or more additive antennas to the existing wideband radar system, which may be the main reason that no practical system appears up to now. It should be significant without doubt if 3-D InISAR imaging could be directly carried out with existing wideband radar, i.e., one-antenna InISAR 3-D imaging.

In this paper, we investigate the feasibility of one-antenna InISAR imaging in theory. First, pulses during three near measurement intervals are selected from the whole track of target, and three ISAR images are obtained. For a short time interval, the time and space decorrelation between different intervals is approximately neglected, which is the basic of our analysis. Then interferometric processing among the three ISAR images is implemented and the azimuth/height coordinates of target are calculated from the interferometric phases and geometrical relationship. The vertical coordinates are obtained from range cell number in ISAR images. Moreover, the target track requirements are discussed. In the end, we present some simulations to validate the theoretical analysis.

2. SIGNAL MODEL

The track of target relative to radar is shown in Fig. 1. The received pulses during three time intervals are selected from the whole track of target, and different means of selection for three intervals are shown in Fig. 2. In fact, both (a) and (b) are special cases of (c) in Fig. 2. In

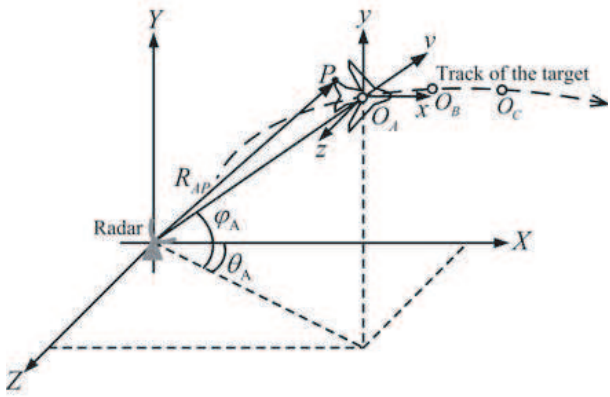

Figure 1. Geometry of the target relative to the radar.

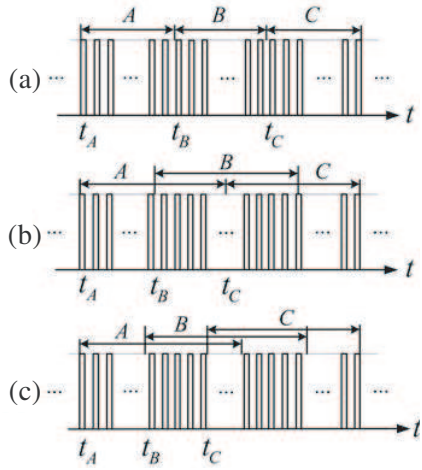

Figure 2. Means of time subsection for three measurement intervals.

the radar observation system, the positions of target at time t_A, t_B, t_C are O_A (R_A, θ_A, φ_A), O_B (R_B, θ_B, φ_B), O_C (R_C, θ_C, φ_C) respectively, as shown in Fig. 1. P is an arbitrary point of the target.

Suppose that the wideband radar transmits chirp signal

$$s\left(\hat{t}, t_m\right) = \text{rect}\left(\frac{\hat{t}}{T_p}\right) \exp\left\{j2\pi\left(f_c t + \gamma \hat{t}^2/2\right)\right\} \tag{1}$$

where rect$(\cdot)$ is the rectangular pulse, f_c is the carrier frequency, T_p is the pulse width, γ is the frequency modulation rate, $\hat{t} = t - mT$ is the fast time, $t_m = mT$ is the slow time, T is the pulse repetition period, $m = 0, 1, 2, \ldots M-1$, and M is the number of total pulses.

Then after the dechirping processing, the normalized base-band echo of scatterer P at time t is [14]

$$\begin{aligned} s_{\text{if}}\left(\hat{t}, t_m\right) \;=\; & \text{rect}\left(\frac{\hat{t} - 2R_P/c}{T_p}\right) \exp\left\{-j\frac{4\pi}{c}\gamma\left(\hat{t} - \frac{2R_{ref}}{c}\right) R_{\Delta P}\right\} \\ & \exp\left\{-j\frac{4\pi}{c} f_c R_{\Delta P}\right\} \exp\left\{j\frac{4\pi\gamma}{c^2} R_{\Delta P}^2\right\} \end{aligned} \tag{2}$$

where $R_{\Delta P} = R_P - R_{ref}$, R_P is the distance between P and radar at time t, R_{ref} is the reference range, and we suppose that $R_{\Delta P}$ is fixed relative to the fast time $\hat{t}$ while changes with the slow time t_m during an imaging period.

By Fourier transform of (2) in terms of $\hat{t} - 2R_{ref}/c$, we obtain

$$S_{\text{if}}(f, t_m) = T_p \operatorname{sinc}\left[T_p\left(f + \frac{2\gamma}{c}R_{\Delta P}\right)\right] \exp\left\{-j\frac{4\pi}{\lambda}R_{\Delta P}\right\} \exp\left\{-j\frac{4\pi f}{c}R_{\Delta P}\right\} \exp\left\{-j\frac{4\pi\gamma}{c^2}R_{\Delta P}^2\right\} \quad (3)$$

where $\operatorname{sinc}(a) = \sin(\pi a)/\pi a$, and λ is the wavelength of the transmitted signal.

During a short time interval, changes of $R_{\Delta P}$ are nearly linear, i.e., $R_{\Delta P} \approx R_{\Delta P0} + V_P t_m$, where $R_{\Delta P0}$ is the distance between P and the reference point initially. After motion compensation and removing the last two terms in (3) [14], we have

$$S(f,t_m) = T_p \operatorname{sinc}\left[T_p\left(f + \frac{2\gamma}{c}R_{\Delta P0}\right)\right] \exp\left\{-j\frac{4\pi}{\lambda}(R_{\Delta P0} + V_P t_m)\right\} \operatorname{rect}\left(\frac{t_m}{T_1}\right) \quad (4)$$

where T_1 is the total time interval during an imaging period.

By Fourier transform of (4) in terms of t_m, we have

$$S(f, f_m) = T_p T_1 \operatorname{sinc}\left[T_p\left(f + \frac{2\gamma}{c}R_{\Delta P0}\right)\right] \operatorname{sinc}\left[T_1\left(f_m + \frac{2V_P}{\lambda}\right)\right] \exp\left\{-j\frac{4\pi}{\lambda}R_{\Delta P0}\right\} \quad (5)$$

From (5), we can obtain the complex ISAR images of scatterer P for time intervals A, B, C respectively

$$S_A(f, f_m) = T_p T_1 \operatorname{sinc}\left[T_p\left(f + \frac{2\gamma}{c}R_{\Delta AP0}\right)\right] \operatorname{sinc}\left[T_1\left(f_m + \frac{2V_{AP}}{\lambda}\right)\right] \exp\left\{-j\frac{4\pi}{\lambda}R_{\Delta AP0}\right\} \quad (6)$$

$$S_B(f, f_m) = T_p T_1 \operatorname{sinc}\left[T_p\left(f + \frac{2\gamma}{c}R_{\Delta BP0}\right)\right] \operatorname{sinc}\left[T_1\left(f_m + \frac{2V_{BP}}{\lambda}\right)\right] \exp\left\{-j\frac{4\pi}{\lambda}R_{\Delta BP0}\right\} \quad (7)$$

$$S_C(f, f_m) = T_p T_1 \operatorname{sinc}\left[T_p\left(f + \frac{2\gamma}{c}R_{\Delta CP0}\right)\right] \operatorname{sinc}\left[T_1\left(f_m + \frac{2V_{CP}}{\lambda}\right)\right] \exp\left\{-j\frac{4\pi}{\lambda}R_{\Delta CP0}\right\} \quad (8)$$

where $R_{\Delta AP0}$, $R_{\Delta BP0}$, $R_{\Delta CP0}$ are respectively the distances between P and the reference point at t_A, t_B, t_C, and V_{AP}, V_{BP}, V_{CP}

are the corresponding average change rate of $R_{\Delta P}$ during time intervals A, B, C.

When the observation time interval is short and the view angle is small in the far field, we can select any two ISAR images among A, B, C to perform interferometric processing in principle. Here we select ISAR image of B to perform interferometric processing with the other two ISAR images. After image registration and interferometric processing, the interferometric phase differences of P are

$$\begin{aligned}\Delta\varphi_{BA} &= \text{Angle}\left(S_B^*(f,f_m)S_A(f,f_m)\right)\\ &= \frac{4\pi}{\lambda}(R_{\Delta BP0}-R_{\Delta AP0}) \triangleq \frac{4\pi}{\lambda}\Delta R_{BA0} \qquad (9)\\ \Delta\varphi_{BC} &= \text{Angle}\left(S_B^*(f,f_m)S_C(f,f_m)\right)\\ &= \frac{4\pi}{\lambda}(R_{\Delta BP0}-R_{\Delta CP0}) \triangleq \frac{4\pi}{\lambda}\Delta R_{BC0} \qquad (10)\end{aligned}$$

where operator Angle$(\cdot)$ returns the phase angles for each element of a complex matrix.

3. 3-D IMAGING ALGORITHM

Although the one-antenna interferometric processing proposed in Section 2 is similar to that of traditional three-antenna InISAR, the "equivalent baseline" can not be measured directly. Therefore the azimuth/height information of target can not be obtained by traditional methods [8]. Then we will propose a method to acquire the scatterer position information from interferometric phases in (9)–(10).

3.1. Coordinate Transform

We introduce a coordinate transform (CT) process, so that the target center O_A at time t_A lies on the vertical coordinate of the transformed radar coordinate system, which is called radar LOS coordinate system here.

As shown in Fig. 3, the radar LOS coordinate system UVW is equivalent to be acquired by carrying out twice CT processes from the radar rectangular coordinate system XYZ.

First, take Y as an axis and rotate XOZ clockwise by θ_A to $X'OZ'$, with the rotation matrix being

$$\mathbf{M_1} = \begin{bmatrix}\cos\theta_A & 0 & \sin\theta_A\\ 0 & 1 & 0\\ -\sin\theta_A & 0 & \cos\theta_A\end{bmatrix} \qquad (11)$$

Then, take Z' as an axis and rotate YOX' clockwise by $\pi/2-\varphi_A$ to $Y''OX''$, with the rotation matrix being

$$\mathbf{M}_2=\begin{bmatrix}\cos(\pi/2-\varphi_A) & -\sin(\pi/2-\varphi_A) & 0\\ \sin(\pi/2-\varphi_A) & \cos(\pi/2-\varphi_A) & 0\\ 0 & 0 & 1\end{bmatrix}=\begin{bmatrix}\sin\varphi_A & -\cos\varphi_A & 0\\ \cos\varphi_A & \sin\varphi_A & 0\\ 0 & 0 & 1\end{bmatrix} \quad (12)$$

Hence, we obtain the radar LOS coordinate system $X''Y''Z'$, i.e., UVW, where the vertical axis is just in the LOS direction.

As a result, the total circumrotation matrix is

$$\mathbf{M}=\mathbf{M_2}\mathbf{M_1}=\begin{bmatrix}\sin\varphi_A\cos\theta_A & -\cos\varphi_A & \sin\varphi_A\sin\theta_A\\ \cos\varphi_A\cos\theta_A & \sin\varphi_A & \cos\varphi_A\sin\theta_A\\ -\sin\theta_A & 0 & \cos\theta_A\end{bmatrix} \quad (13)$$

Suppose the target position in coordinate system XYZ is (X, Y, Z), then the corresponding coordinates in coordinate system UVW is

$$\begin{pmatrix}U\\V\\W\end{pmatrix}=\mathbf{M}\begin{pmatrix}X\\Y\\Z\end{pmatrix}=\begin{bmatrix}\sin\varphi_A\cos\theta_A & -\cos\varphi_A & \sin\varphi_A\sin\theta_A\\ \cos\varphi_A\cos\theta_A & \sin\varphi_A & \cos\varphi_A\sin\theta_A\\ -\sin\theta_A & 0 & \cos\theta_A\end{bmatrix}\begin{pmatrix}X\\Y\\Z\end{pmatrix} \quad (14)$$

Specially, target positions in coordinate system UVW at time t_A, t_B, t_C are respectively (U_A, V_A, W_A), (U_B, V_B, W_B), (U_C, V_C, W_C).

3.2. 3-D Geometric Position Determination

As illustrated in Fig. 3, a local coordinate system uvw parallel to the radar LOS coordinate system is used to describe the positions of the scatterers on the target. The target center, which is also origin of

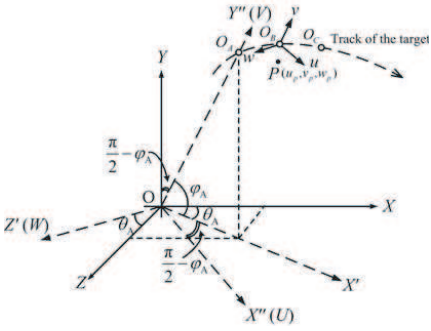

Figure 3. Coordinate transform from radar rectangular coordinate system to radar LOS coordinate system.

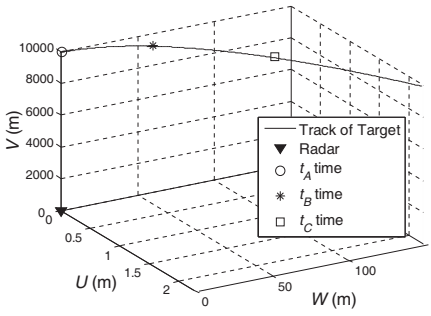

Figure 4. Target track.

the local coordinate system, is located at (U, V, W) in the radar LOS coordinate system. Point P located at (u_p, v_p, w_p) in local coordinate system is expressed as $\vec{P}$, corresponding to $(U+u_p, V+v_p, W+w_p)$ in radar LOS coordinate system. In particular, the coordinates of P in radar LOS coordinate system are respectively P_A $(U_A+u_p, V_A+v_p, W_A+w_p)$, P_B $(U_B+u_p, V_B+v_p, W_B+w_p)$, P_C $(U_C+u_p, V_C+v_p, W_C+w_p)$ at t_A, t_B, t_C.

In terms of the geometry depicted in Fig. 3, we have

$$OO_A = \left|\overrightarrow{OA}\right| = \left[U_A^2 + V_A^2 + W_A^2\right]^{1/2} \tag{15}$$

$$OO_B = \left|\overrightarrow{OB}\right| = \left[U_B^2 + V_B^2 + W_B^2\right]^{1/2} \tag{16}$$

$$OO_C = \left|\overrightarrow{OC}\right| = \left[U_C^2 + V_C^2 + W_C^2\right]^{1/2} \tag{17}$$

$$OP_A = \left|\overrightarrow{OA} + \vec{P}\right| = \left[(U_A+u_p)^2 + (V_A+v_p)^2 + (W_A+w_p)^2\right]^{1/2} \tag{18}$$

$$OP_B = \left|\overrightarrow{OB} + \vec{P}\right| = \left[(U_B+u_p)^2 + (V_B+v_p)^2 + (W_B+w_p)^2\right]^{1/2} \tag{19}$$

$$OP_C = \left|\overrightarrow{OC} + \vec{P}\right| = \left[(U_C+u_p)^2 + (V_C+v_p)^2 + (W_C+w_p)^2\right]^{1/2} \tag{20}$$

We choose the distance between radar and target center as the reference range for each pulse in the dechirping processing, and in the far field we have $OP_A \approx OP_B \approx OP_C \approx OO_A \approx OO_B \approx OO_C \approx \tilde{R}$, $\overrightarrow{OA}/|\overrightarrow{OA}| \approx \overrightarrow{n_0}$, $OO_B - OP_B \approx -\vec{P}^T\overrightarrow{n_0}$, $OO_A - OP_A \approx -\vec{P}^T\overrightarrow{n_0}$. Then

$$\begin{aligned}
&R_{\Delta BP0} - R_{\Delta AP0} \\
&= (OP_B - OO_B) - (OP_A - OO_A) = \frac{OP_B^2 - OP_A^2}{OP_B + OP_A} - \frac{OO_B^2 - OO_A^2}{OO_B + OO_A} \\
&= \frac{(\overrightarrow{OB} + \vec{P})^T(\overrightarrow{OB}+\vec{P}) - (\overrightarrow{OA}+\vec{P})^T(\overrightarrow{OA} + \vec{P})}{OP_B + OP_A} - \frac{\overrightarrow{OB}^T\overrightarrow{OB} - \overrightarrow{OA}^T\overrightarrow{OA}}{OO_B + OO_A} \\
&= \frac{\overrightarrow{OB}^T\overrightarrow{OB} - \overrightarrow{OA}^T\overrightarrow{OA} + 2\overrightarrow{AB}^T\vec{P}}{OP_B + OP_A} - \frac{\overrightarrow{OB}^T\overrightarrow{OB} - \overrightarrow{OA}^T\overrightarrow{OA}}{OO_B + OO_A} \\
&= \frac{\left(\overrightarrow{OB}^T\overrightarrow{OB} - \overrightarrow{OA}^T\overrightarrow{OA}\right)(OO_B + OO_A - OP_B - OP_A)}{(OP_B + OP_A)(OO_B + OO_A)} + \frac{2\overrightarrow{AB}^T\vec{P}}{OP_B + OP_A} \\
&= \frac{(OO_B + OO_A)(\overrightarrow{AB}^T\overrightarrow{n_0})(-2\vec{P}^T\overrightarrow{n_0})}{(OP_B + OP_A)(OO_B + OO_A)} + \frac{2\overrightarrow{AB}^T\vec{P}}{OP_B + OP_A} \\
&= \frac{(\overrightarrow{AB} - (\overrightarrow{AB}^T\overrightarrow{n_0})\overrightarrow{n_0})^T\vec{P}}{\tilde{R}}
\end{aligned} \tag{21}$$

After the CT process indicated in Section 3.1, the target center O_A at time t_A lies on the vertical coordinate of radar LOS coordinate system, therefore $U_A = 0$, $W_A = 0$, and

$$\overrightarrow{n_0} \approx \overrightarrow{OA} / \left|\overrightarrow{OA}\right| = [U_A, V_A, W_A]^T / \left[U_A^2 + V_A^2 + W_A^2\right]^{1/2} = [0, 1, 0]^T \quad (22)$$

So

$$\begin{aligned} \overrightarrow{AB} - (\overrightarrow{AB}^T \overrightarrow{n_0})\overrightarrow{n_0} &= [U_B - U_A, V_B - V_A, W_B - W_A]^T - (V_B - V_A)[0, 1, 0]^T \\ &= [U_B - U_A, 0, W_B - W_A]^T \end{aligned} \quad (23)$$

Substituting (23) into (21), we have

$$\begin{aligned} R_{\Delta BP0} - R_{\Delta AP0} &= [U_B - U_A, 0, W_B - W_A](u_p, v_p, w_p)^T / \tilde{R} \\ &= ((U_B - U_A)u_p + (W_B - W_A)w_p)/\tilde{R} \end{aligned} \quad (24)$$

Similarly, we also have

$$\begin{aligned} R_{\Delta BP0} - R_{\Delta CP0} &= \frac{(\overrightarrow{CB} - (\overrightarrow{CB}^T \overrightarrow{n_0})\overrightarrow{n_0})^T \vec{P}}{\tilde{R}} \\ &= ((U_B - U_C)u_p + (W_B - W_C)w_p)/\tilde{R} \end{aligned} \quad (25)$$

Substituting (24)–(25) into (9)–(10), we have

$$\Delta\varphi_{BA} = \frac{4\pi}{\lambda}(R_{\Delta BP0} - R_{\Delta AP0}) = \frac{4\pi}{\lambda}\left\{\frac{1}{\tilde{R}}[(U_B - U_A)u_P + (W_B - W_A)w_P]\right\} \quad (26)$$

$$\Delta\varphi_{BC} = \frac{4\pi}{\lambda}(R_{\Delta BP0} - R_{\Delta CP0}) = \frac{4\pi}{\lambda}\left\{\frac{1}{\tilde{R}}[(U_B - U_C)u_P + (W_B - W_C)w_P]\right\} \quad (27)$$

From (26)–(27), we have

$$\mathbf{R}\begin{bmatrix} u_P \\ w_P \end{bmatrix} = \mathbf{Q} \quad (28)$$

where $\mathbf{R} = \begin{bmatrix} U_B - U_A & W_B - W_A \\ U_B - U_C & W_B - W_C \end{bmatrix}$, $\mathbf{Q} = \begin{bmatrix} \Delta\varphi_{BA}\lambda\tilde{R}/4\pi \\ \Delta\varphi_{BC}\lambda\tilde{R}/4\pi \end{bmatrix}$.

When $\mathbf{R}$ is not a singular matrix, i.e., $\det(\mathbf{R}) \neq 0$

$$\begin{bmatrix} u_P \\ w_P \end{bmatrix} = \mathbf{R}^{-1}\mathbf{Q} \quad (29)$$

Generally, v_P can be determined from the range cell number of each scatterer in ISAR images. So far, all the 3-D spatial positions of each scatterer on the target are acquired, and the 3-D image is obtained considering the corresponding relationship of 3-D coordinates accordingly.

It is worth noting that $\det(\mathbf{R}) \neq 0$ is a premise for one-antenna 3-D InISAR imaging. Now we study the inherent physical meaning. From

$\det(\mathbf{R}) = 0$, we have $OV||O_AO_BO_C$ plane or three points O_A, O_B, O_C are collinear. The detailed derivation can be found in Appendix A. It is obvious that when the target moves along a straight line or the target track plane is parallel to the LOS direction, $\mathbf{R}$ is a singular matrix and the coordinates in (29) can not be computed. In other words, when the target moves in a line that deviates from straightness and the target track plane is not parallel to the LOS direction, one-antenna InISAR 3-D imaging is feasible.

4. SIMULATIONS

To validate the proposed one-antenna InISAR 3-D imaging method, the far-field moving target with a curvilinear track is imaged based on one-antenna geometry, and the target is located initially 10 km away from the origin as shown in Fig. 4. The velocity of target is 50 m/s. The whole observation time is 3 s, and the target positions measured in radar coordinate system XYZ during the observation time is shown in Fig. 5. Chirp pulses are transmitted, and the radar carrier frequency is 10 GHz. The pulse repetition frequency (PRF) is 100 Hz, and the bandwidth is 1 GHz, giving a down-range resolution of 0.15 m. The target is a simple aircraft model, as shown in Fig. 6. We select the means of time subsection for ISAR imaging illustrated in Fig. 2(a), so $t_A = 0$ s, $t_B = 1$ s, $t_C = 2$ s, and there are 100 pulses during each time interval respectively.

ISAR imaging result for time interval A is shown in Fig. 7. The ISAR imaging results for time interval B and C are similar to that for time interval A. The vertical coordinates v_P for a certain scatterer can be determined from the range cell number in ISAR images.

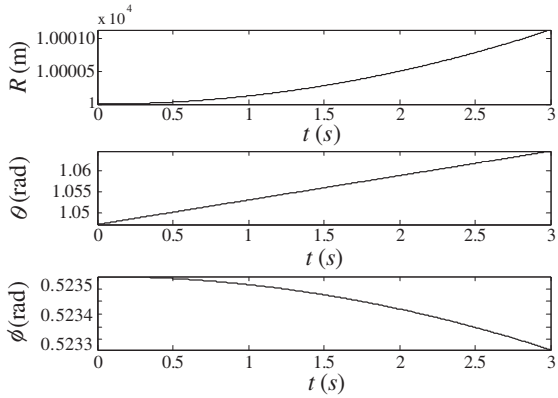

Figure 5. Target positions during the observation time (range, azimuth, pitching).

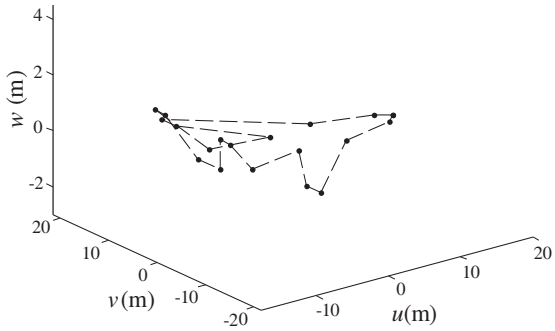

Figure 6. 3-D view of target model.

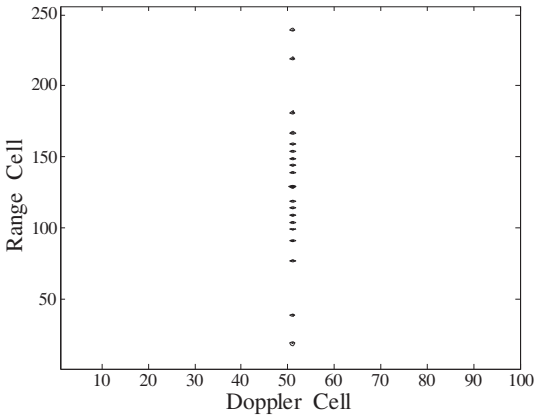

Figure 7. ISAR imaging result.

The one-antenna InISAR 3-D imaging results, obtained with the imaging algorithm presented in Section 3, are given in Fig. 8. For convenience of comparison, the actual scatterer distribution (hollow circle) and the imaging results (solid dot) are drawn in the same figure. It is obvious that the estimated 3-D coordinates are consistent with the actual target model on the whole, so the proposed one-antenna InISAR imaging method is effective.

It is worth noting that the cross-range resolution is poor for the designed curvilinear track, and the scatterers can not be effectively resolved along the Doppler direction. As a result, the ISAR image in Fig. 7 occupies only one Doppler cell. Fortunately, the resulting 3-D image is not much influenced in our simulation due to the simple structure of the target, and the more complicated cases will be a topic for our future study.

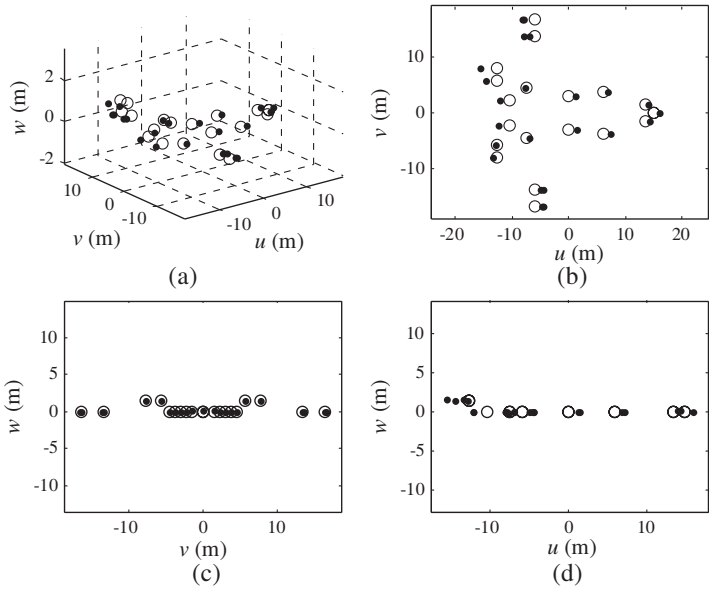

Figure 8. Comparison between one-antenna InISAR 3-D imaging results (solid dot) and actual scatterer model (hollow circle). (a) 3-D imaging result. (b) Projection of the image on the u-v plane. (c) Projection of the image on the v-w plane. (d) Projection of the image on the u-w plane.

5. CONCLUSIONS

In this paper, we proposed an InISAR 3-D imaging method using only one antenna. Three ISAR images obtained at different but near time intervals are used to perform interferometric processing and target coordinates are estimated from the interferometric phases. The proposed algorithm depends on the target track. When the target moves along a line that is not straight and the target track plane is not parallel to the LOS direction, one-antenna InISAR 3-D imaging is feasible. Simulations verified the effectiveness of the proposed method.

As a remark, there are some difficulties to achieve InISAR imaging using only one antenna in practical application: 1) the track of non-cooperative target is out of control, so the premise of one-antenna InISAR is not always guaranteed; 2) the proposed method requires a high real-time measure precision of target position parameters (range, azimuth, pitching); 3) the curve track of target sometimes degrades the ISAR imaging quality and the correlation between different ISAR images. In despite of these difficulties, it is still of great significance for

our work because the proposed one-antenna InISAR imaging method can be carried out directly on the existing wideband radar without additive antennas and reduces the hardware complexity.

ACKNOWLEDGMENT

This work was supported by the China National Funds for Distinguished Young Scientists under Grants 61025006. The authors would like to thank the anonymous reviewers and the editors for improving the manuscript.

APPENDIX A.

In this Appendix, we study the physical meaning of $\det(\mathbf{R}) = 0$ in Section 3.2.

From $\det(\mathbf{R}) = \begin{vmatrix} U_B - U_A & W_B - W_A \\ U_B - U_C & W_B - W_C \end{vmatrix} = 0$, we have $(U_B - U_A)(W_B - W_C) = (W_B - W_A)(U_B - U_C)$, and then all the possible cases are given below:

1) $U_B - U_A = 0, W_B - W_A = 0 \Rightarrow O_AO_B||OV \Rightarrow OV||O_AO_BO_C$ plane;
2) $U_B - U_A = 0$, $U_B - U_C = 0 \Rightarrow U_A = U_B = U_C \Rightarrow O_AO_BO_C$ plane $||VOW$ plane $\Rightarrow OV||O_AO_BO_C$ plane;
3) $W_B - W_C = 0, W_B - W_A = 0 \Rightarrow W_A = W_B = W_C \Rightarrow O_AO_BO_C$ plane $||VOU$ plane $\Rightarrow OV||O_AO_BO_C$ plane;
4) $W_B - W_C = 0$, $U_B - U_C = 0 \Rightarrow O_BO_C||OV \Rightarrow OV||O_AO_BO_C$ plane;
5) $\frac{U_B - U_A}{W_B - W_A} = \frac{U_B - U_C}{W_B - W_C}$, $U_B - U_A \neq 0$, $W_B - W_A \neq 0$, $U_B - U_C \neq 0$, $W_B - W_C \neq 0 \Rightarrow O_A, O_B, O_C$ are collinear.

where the symbol "||" denotes "be parallel to".

Therefore, from $\det(\mathbf{R}) = 0$, we have $OV \| O_AO_BO_C$ plane or three points O_A, O_B, O_C are collinear.

REFERENCES

1. Wehner, D. R., *High-resolution Radar*, 2nd edition, Artech House, Boston, 1995.
2. Ma, C. Z., "Research on radar target three-dimensional imaging," Xidian University, Xi'an, 1999.
3. Zhang, D. C., "Research on the key techniques of interferometric inverse synthetic aperture radar imaging," University of Science and Technology of China, Hefei, 2009.

4. Wang, G. Y., X. G. Xia, and V. C. Chen, "Three-dimensional ISAR imaging of maneuvering targets using three receivers," *IEEE Transactions on Image Processing*, Vol. 10, No. 3, 436–447, 2001.
5. Zhang, Q., C. Z. Ma, T. Zhang, and S. H. Zhang, "Research on 3-D imaging technique for interferometric inverse synthetic aperture radar," *Journal of Electronics & Information Technology*, Vol. 23, No. 9, 890–898, 2001.
6. Xu, X. J. and R. M. Narayanan, "Three-dimensional interferometric ISAR imaging for target scattering diagnosis and modeling," *IEEE Transactions on Image Processing*, Vol. 10, No. 7, 1094–1102, 2001.
7. Zhang, Q. and T. S. Yeo, "Three-dimensional SAR imaging of a ground moving target using the InISAR technique," *IEEE Transactions on Geoscience and Remote Sensing*, Vol. 42, No. 9, 1818–1828, 2004.
8. Zhang, Q., T. S. Yeo, G. Du, and S. H. Zhang, "Estimation of three-dimensional motion parameters in interferometric ISAR imaging," *IEEE Transactions on Geoscience and Remote Sensing*, Vol. 42, No. 2, 292–300, 2004.
9. Given, J. A. and W. R. Schmidt, "Generalized ISAR-part II: Interferometric techniques for three-dimensional location of scatterers," *IEEE Transactions on Image Processing*, Vol. 14, No. 11, 1792–1797, 2005.
10. Ma, C. Z., T. S. Yeo, H. S. Tan, and G. Lu, "Interferometric ISAR imaging on squint model," *Progress In Electromagnetics Research Letters*, Vol. 2, 125–133, 2008.
11. Kostis, T. G., K. G. Galanis, and S. K. Katsikas, "Angular glint effects generation for false naval target verisimility requirements," *Measurement Science and Technology*, 1–13, 2009.
12. Zhang, D. C., D. J. Wang, and W. D. Chen, "An InISAR 3-D imaging method based on joint cross-time-frequency distribution," *Acta Electronica Sinica*, Vol. 37, No. 4, 833–838, 2009.
13. Soumekh, M., "Automatic aircraft landing using interferometric inverse synthetic aperture radar imaging," *Proc. International Conference on Image Processing*, 23–26, 1995.
14. Bao, Z., M. Xing, and T. Wang, *Radar Imaging Approaches*, 24–30, Publishing House of Electronics Industry, Beijing, 2005.